Journal of Fluids and Structures (2001) **15,** 513–521
doi:10.1006/jfls.2000.0357, available online at http://www.idealibrary.com on IDEAL®

A CFD STUDY OF THE DYNAMIC RESPONSE OF A ROTATING CYLINDER IN A CURRENT

P. K. STANSBY

Department of Civil and Construction Engineering, UMIST
Manchester M60 1QD, U.K.

AND

R. C. T. RAINEY†

Centre for Nonlinear Dynamics, University College London
Gower Street, London WC1E 6BT, U.K.

(Received 28 September 2000, and in final form 15 November 2000)

A new form of dynamic response for a flexibly mounted, rotating cylinder in a current, as observed in experiments, has been investigated through 2-D, laminar CFD. Orbital response of opposite rotation to that of the cylinder and with amplitudes of several diameters can occur with a maximum at $\alpha = 0{\cdot}3$, where α is the ratio of current velocity to rotation speed of the cylinder surface. Instantaneous flows and forces for this α value are related to those for a nonresponding cylinder but it is shown that the forcing is far from quasi-steady and is due to rapidly changing wake structures during part of a cycle.

1. INTRODUCTION

FOR DEEP-WATER offshore oil exploration, the possibility of using a drillstring without an outer casing is of operational interest. It poses the hydrodynamic problem of a flexibly mounted rotating cylinder in a current. To investigate this, simple experiments with a lightly damped rotating cylinder in a current and computational fluid dynamics (CFD) have been undertaken.

A new form of orbital response was observed in the experiments. It is mainly dependent on the ratio, α, of current velocity, U_{cur}, to cylinder surface velocity, U_{rot}, and the reduced velocity, $V_r = U_{\text{cur}}/f_n D$, where f_n is the natural frequency in water and D is the diameter. Low-frequency response with an amplitude of several diameters can occur with $0{\cdot}25 < \alpha < 0{\cdot}5$, the orbital rotation being of opposite sense to the cylinder rotation, and high-frequency response of small amplitude, with orbital rotation of the same sense, may be superimposed, becoming more noticeable as α decreases. Elementary potential-flow analysis consistently predicts that there will be two natural periods of orbital oscillation: one larger than the structural natural period and one smaller. This analysis combined with empirical estimates of the Magnus force gave approximate predictions of the oscillation frequencies observed. The analysis does not, however, explain the origin of the hydrodynamic mechanisms causing the response to occur. In order to understand this, a 2-D

† Also with W. S. Atkins Ltd., Berkshire House, 171 High Holborn, London WC1V 7AA, U.K.

0889–9746/01/040513 + 09 $35.00/0

computational study has been undertaken where streamline and vorticity plots may be related to response and force time histories. Such numerical simulation is now quite reliable for unsteady, laminar flow which, in 2-D, may be undertaken on modern workstations. The finite-volume code of Lien & Leschziner (1994) has been adapted for cylinder flows (Cobbin *et al.* 1998) and further modified to allow dynamic response by modifying the outer boundary conditions to define the velocity relative to the cylinder and the pressure gradient with the effect of relative flow acceleration. The resulting computed force includes a Froude–Krylov component which must be subtracted to correspond with the force in the experimental conditions. Values of mass, damping and natural frequency typical of the practical situation are chosen: the cylinder mass is given a relative density of 2·83, the logarithmic decrement of damping $\delta = 0{\cdot}01$ and $V_r = 14$. A Reynolds number $\mathrm{Re}_{\mathrm{cur}} = U_{\mathrm{cur}} D/\nu = 200$ (ν is kinematic viscosity) was chosen for the dynamic simulations as this is approximately the largest value (for nonrotating cylinders) which allows 2-D flow, before 3-D effects appear. This is an order of magnitude lower than that in the experiments which is an order of magnitude lower than in the offshore problem.

The mass-spring-damper system defining the displacements with two degrees of freedom, x and y, is given by

$$\begin{aligned} \ddot{x} + 2c\omega_n \dot{x} + \omega_n^2 x - 2c\omega\omega_n y &= F_x/m, \\ \ddot{y} + 2c\omega_n \dot{y} + \omega_n^2 y + 2c\omega\omega_n x &= F_y/m, \end{aligned} \tag{1}$$

where m is the mass per unit length, F_x, F_y are forces per unit length in the x- and y-directions, ω is the angular rotation (clockwise) speed of the cylinder, ω_n and c are the structural natural frequency and damping ratio in vacuo/air (although the value of f_n in water is used to define V_r). Note the additional cross-coupling effect due to cylinder rotation (Bishop 1959).

It is the intention of this note to summarize some of the CFD results which give insight into the origin of the response where it is a maximum. Further detailed description, including experiments, potential-flow analysis and CFD, will be given in Stansby & Rainey (2001).

2. RESULTS

It is first important to known how the flow around a rotating cylinder which is not responding depends on α. Figure 1 shows streamline plots with $\mathrm{Re}_{\mathrm{cur}} = 200$ and $\alpha = 0{\cdot}2$, $0{\cdot}25$, $0{\cdot}3$, $0{\cdot}5$ and $1{\cdot}0$. For $\alpha = 0{\cdot}2$, the stagnation point is detached from the cylinder surface (and on the y-axis); the streamlines are similar to those of a point vortex in a uniform stream. For $\alpha = 0{\cdot}25$ the stagnation point has moved closer the cylinder surface and a steady wake has started to form with $\alpha = 0{\cdot}3$. Note that the stagnation point never actually reaches the surface due to the surface velocity. For $\alpha = 0{\cdot}5$, the wake has increased in size but remains attached, fluctuating slightly about a mean position. For $\alpha = 1$, vortex shedding has become established, generating fluctuating lift and drag forces as shown in Figure 1(f). The dependence of these flows on α is consistent with the early experimental visualisations shown in Prandtl & Tietjens (1934).

Computed variations of mean lift and drag with α are shown in Figure 2 with $\mathrm{Re}_{\mathrm{cur}} = 200$ and 10^3, where drag coefficient is defined in the usual way, $C_D = \mathrm{drag}/(0{\cdot}5\,\rho U_{\mathrm{cur}}^2 D)$, and lift coefficient is defined as the fraction of the inviscid Magnus force, $c_L = \mathrm{lift}/(\rho U_{\mathrm{cur}} \Gamma)$ where $\Gamma = \pi D U_{\mathrm{rot}}$ and ρ is water density. From the present computations, for small α, C_D is very small and $c_L \to 1$ as $\alpha \to 0$, in agreement with the theoretical (asymptotic) analysis of Moore (1957).

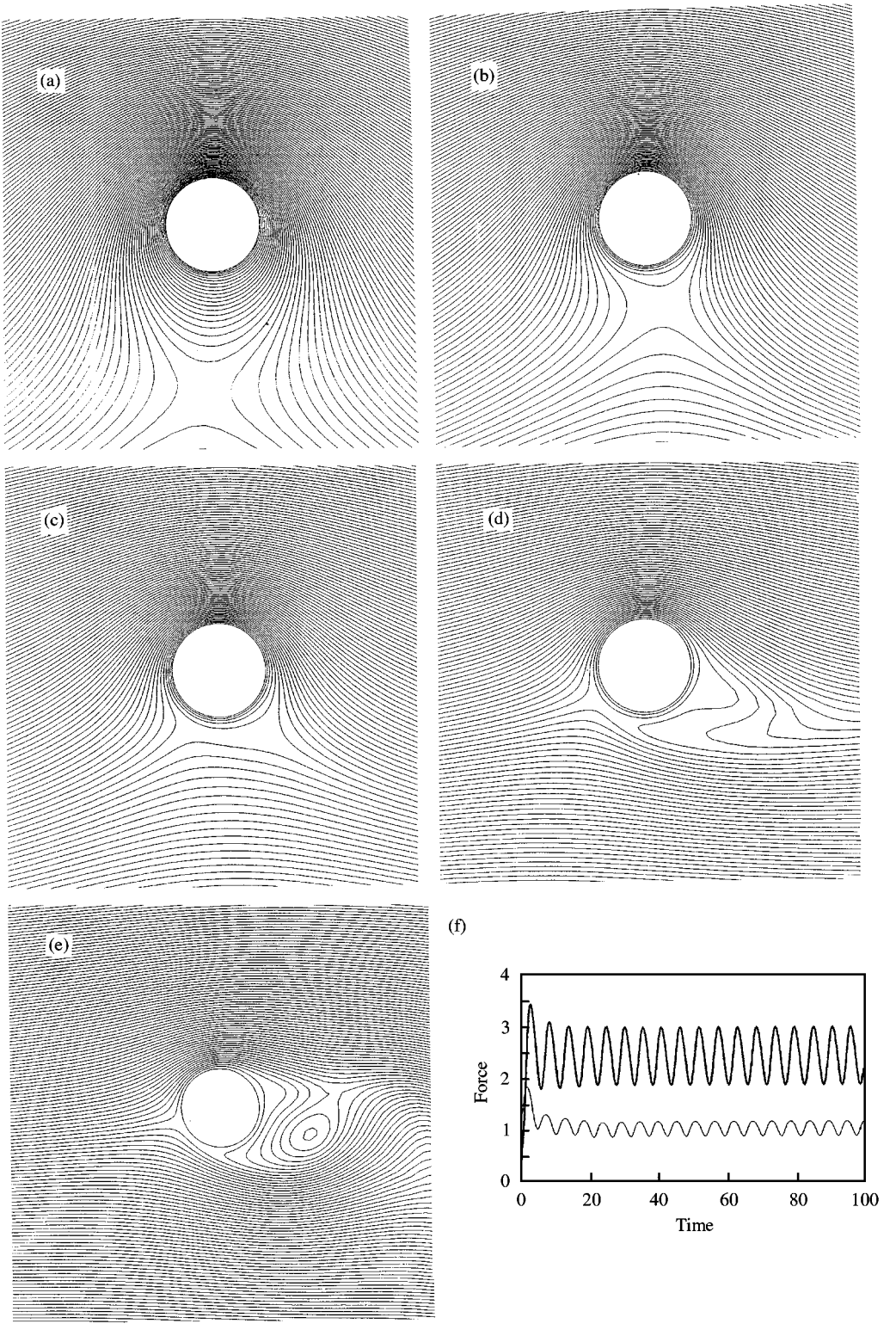

Figure 1. Computed streamline plots for a nonresponding rotating cylinder with $Re_{cur} = 200$:(a) $\alpha = 0{\cdot}2$, (b) $\alpha = 0{\cdot}25$, (c) $\alpha = 0{\cdot}3$, (d) $\alpha = 0{\cdot}5$, (e) $\alpha = 1{\cdot}0$; (f) lift and drag force variation with time for $\alpha = 1{\cdot}0$ (force normalized by $\rho U_{rot}^2 D/2$). Flow is from left to right.

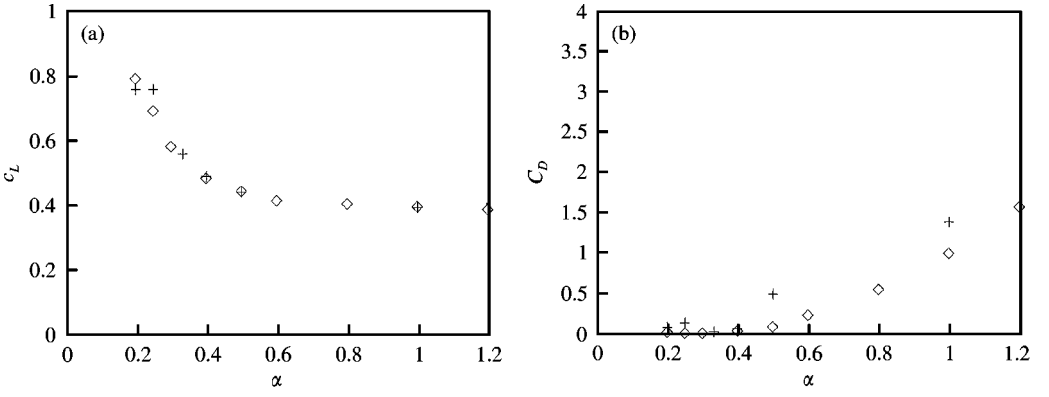

Figure 2. Computed mean force coefficients for a fixed rotating cylinder. (a) c_L variation with α: ◇, $\mathrm{Re}_{\mathrm{cur}} = 200$; +, $\mathrm{Re}_{\mathrm{cur}} = 10^3$. (b) C_D variation with α; notation as in (a).

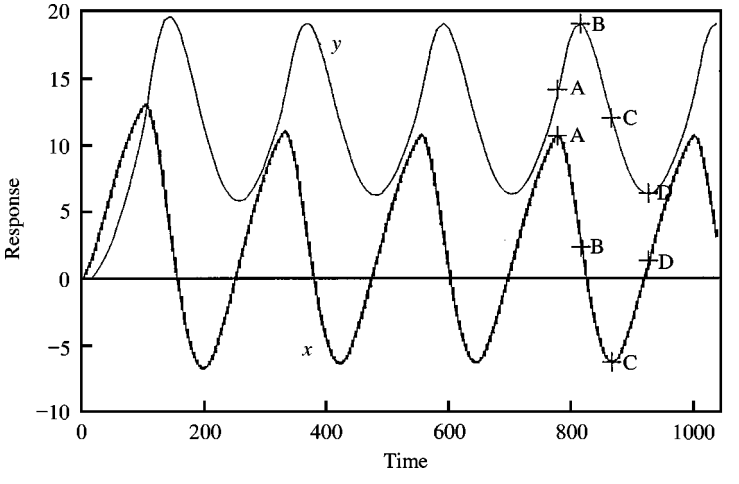

Figure 3. Variation of y/D and x/D with (tU_{rot}/D) for $\bar{\alpha} = 0{\cdot}3$ and $V_r = 14$.

When the cylinder is free to respond (for $tU_{\mathrm{rot}}/D > 5$) with the parameters defined above, x- and y-response variations with time are shown in Figure 3 with the corresponding y versus x plot in Figure 4, showing the orbital nature of the response and some small-amplitude, high-frequency effects. The anticlockwise, large orbital response is of opposite rotation to the clockwise cylinder rotation and the small, high-frequency response is of the same rotation. Points of maximum and minimum x-response are denoted by A and C and of maximum and minimum y-response by B and D. Time variations of force in the x- and y-directions, F_x and F_y, are shown in Figure 5 and can be seen to be in phase with response. The high-frequency force fluctuations are associated with the high-frequency response between A and C.

The "instantaneous" c_L and α due to flow relative to the cylinder are of interest to determine whether quasi-steady assumptions are of value. It is well known, for example, that the flow-induced oscillation known as galloping, resulting from the variation of lift with angle of incidence for noncircular sections, is a quasi-steady phenomenon. Since α is now an instantaneous value $\bar{\alpha}$ is now used to define $U_{\mathrm{cur}}/U_{\mathrm{rot}}$. Instantaneous lift and drag coefficients and α are based on the relative onset velocities: $u_{\mathrm{rel}} = U_{\mathrm{cur}} - \dot{x}$, $v_{\mathrm{rel}} = -\dot{y}$, so

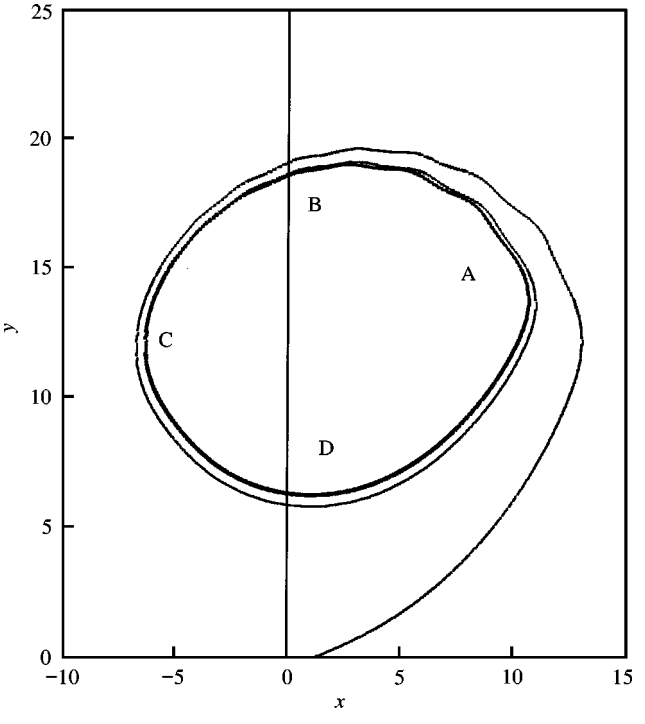

Figure 4. Variations of computed y responses with x, both normalized by D.

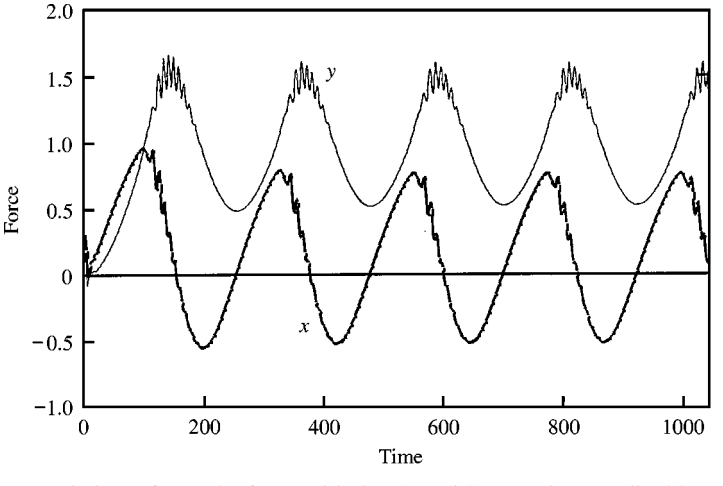

Figure 5. Variations of x- and y-forces with time (tU_{rot}/D). Force is normalized by $\rho U_{rot}^2 D/2$.

that the angle of incidence $\theta = \tan^{-1}(v_{rel}/u_{rel})$ and velocity magnitude $U = \sqrt{u_{rel}^2 + v_{rel}^2}$ gives an instantaneous $\alpha = U/U_{rot}$. The corresponding lift and drag forces transverse to and in line with the instantaneous onset velocity are given by

$$F_L = F_y \cos\theta - F_x \sin\theta,$$
$$F_D = F_x \cos\theta + F_y \sin\theta. \tag{2}$$

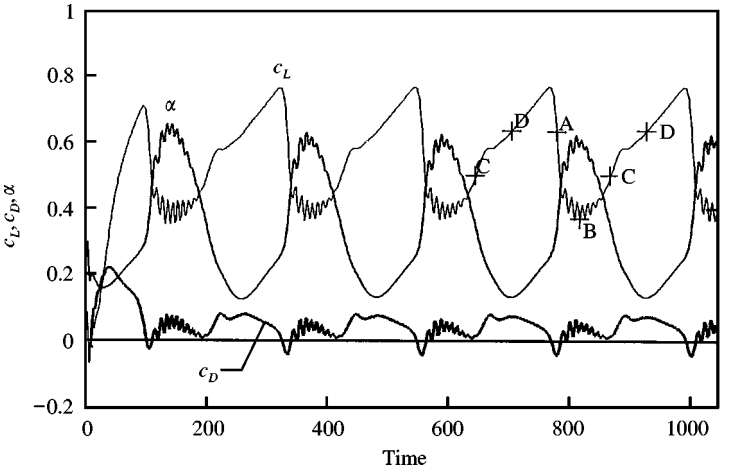

Figure 6. Variations of instantaneous c_L, c_D and α with time (tU_{rot}/D) for $\bar{\alpha} = 0{\cdot}3$ and $V_r = 14{\cdot}0$.

Lift is then normalized so that instantaneous $c_L = F_L/(\rho U \Gamma)$ and c_D (as distinct from C_D) is normalized in the same way for comparison with c_L. Variations of c_L, c_D, and α with time are shown in Figure 6 and points A–D are marked on the c_L curve.

From Figure 6 it is clear that a rapid increase in α around time A coincides with a rapid decrease in c_L. Corresponding streamline and vorticity patterns (for flow relative to the cylinder) are shown in Figure 7 for times $tU_{\text{rot}}/D = 780$, 785, 790 and 795. For "small" α, corresponding to times between C ($tU_{\text{rot}}/D = 647$), and A ($tU_{\text{rot}}/D = 782$), the stagnation point is well below the cylinder, typical of a nonresponding cylinder with $\alpha < 0{\cdot}25$. As α increases rapidly through time A, the stagnation point moves upwards towards the cylinder and an attached wake starts to form soon after time A, at about time 785. By time 790 a wake has formed, associated with a marked decrease in c_L. With high α values around time B the attached wake fluctuates rapidly about some slowly varying position and this is responsible for the high-frequency components in the force variation, the period being about $9D/U_{\text{rot}}$. By time C the wake is about to collapse and the stagnation point move away from the cylinder as the cycle is completed.

Plots of c_L against α are shown in Figure 8 with positions A–D marked. These are plotted for the second half of the time-series where the motion has become periodic. It can be seen that the gradient is generally negative and periodic dynamic response is associated with a pronounced hysteresis loop. It is interesting to see that the high-frequency behaviour is quite repeatable from one cycle to another. The c_L versus α curve effectively defines the response since c_D is small in relation to c_L. Unfortunately, the curve is quite complex and different for each value of $\bar{\alpha}$ [shown in Stansby & Rainey (2001)]. The variation of c_L with α in a cycle is thus far removed from the mean c_L versus α variation for a nonresponding cylinder.

It should be mentioned that these computations are extremely time-consuming. The high-frequency flow structures need to be resolved requiring a small time step while the slow oscillations require long times to cover several cycles. The above run required 4–5 days of computation time (each) on a modern workstation (Dec Alpha 600). A mesh with 80×80 nodes was used with an inner radial mesh spacing of $\sqrt{2\nu\Delta t}$, where Δt is time step (the diffusion length scale), and an outer boundary at $20D$. A time step given by $\Delta t U_{\text{rot}}/D = 0{\cdot}05$ was used. Using a 120×120 mesh with an outer boundary at greater distances showed convergence almost of within plotting accuracy.

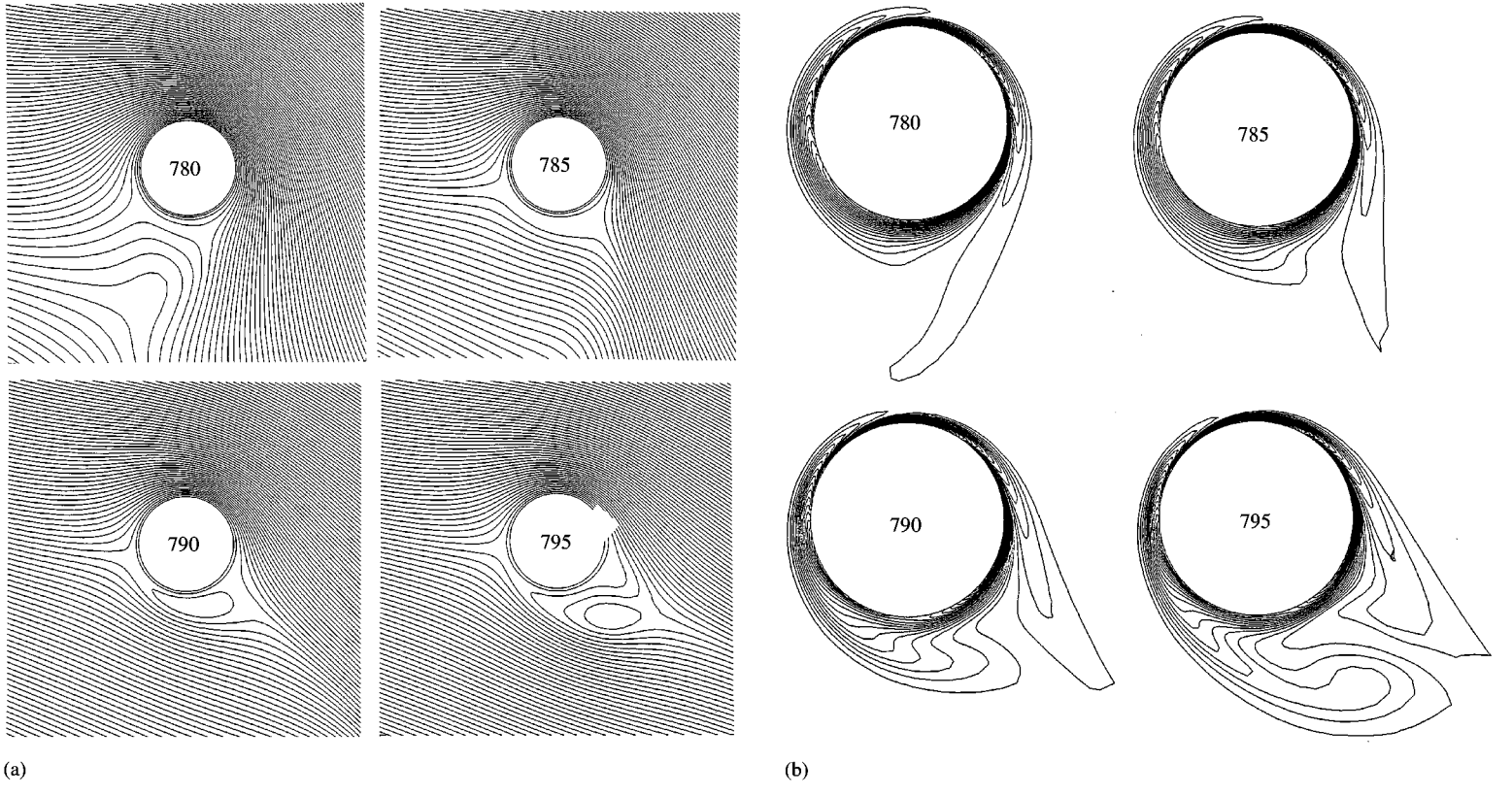

Figure 7. (a) Streamline plots at $tU_{rot}/D = 780$, 785, 790 and 795 (as marked on the figure). The flow is relative to the cylinder. (b) Vorticity plots for (a).

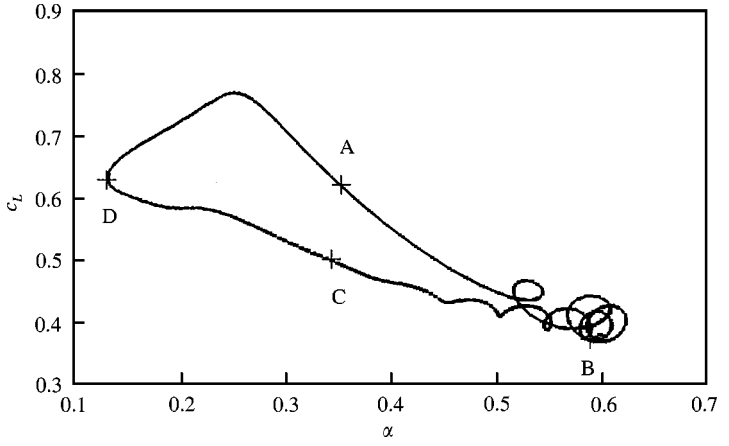

Figure 8. Plots of instantaneous c_L against α.

3. CONCLUSIONS

The large orbital response of opposite rotation to that of the cylinder, observed in experiments, has been qualitatively reproduced by CFD for laminar 2-D flow. Maximum response occurs with $\bar{\alpha} = 0{\cdot}3$ and results for this case with $V_r = 14$ are shown to aid understanding of the hydrodynamic mechanisms causing response. The response and force are shown to be in phase, and there is a rapid decrease in "instantaneous" lift coefficient c_L associated with rapid movement of the stagnation point towards the cylinder, causing wake formation. This is associated with a rapid increase in instantaneous α. As the cycle progresses, wake formation eventually ceases and the stagnation point moves away from the cylinder; α decreases and c_L increases until the dramatic changes noted above are repeated. There is some similarity with flows for a nonresponding cylinder at different (constant) $\bar{\alpha}$ values. However, the plot of c_L versus α shows that the forcing is far from quasi-steady with pronounced hysteresis. High-frequency, small-amplitude response is superimposed for part of the cycle; both the low- and high-frequency responses are consistent with elementary potential-flow analysis. A more general description and analysis is given in Stansby & Rainey (2001).

ACKNOWLEDGEMENTS

This work was supported on a contract from Conoco (US) while the first author was at the Victoria University of Manchester.

REFERENCES

BISHOP, R. E. D. 1959 The vibration of rotating shafts. *IMechE. Journal of Mechanical Engineering Sciences* **1,** 50–65.

COBBIN, A. M., STANSBY, P. K. & LESCHZINER, M. A. 1998 Modelling oscillatory flow around a cylinder using a RANS scheme. In *Proceedings of the ASME Conference on Offshore Mechanics and Arctic Engineering*, Lisbon.

LIEN, F. S. & LESCHZINER, M. A. 1994 A general non-orthogonal finite-volume algorithm for turbulent flows at all speeds incorporating second-moment closure. Part 1. Numerical implementation. *Computational Methods in Applied Mechanics and Engineering* **114,** 123–148.

MOORE, D. W. 1957 The flow past a rapidly rotating circular cylinder in a uniform stream. *Journal of Fluid Mechanics* **2,** 541–550.

PRANDTL, L. & TIETJENS, O. G. 1934 *Applied Hydro- and Aeromechanics.* New York: McGraw Hill.

STANSBY, P. K. & RAINEY, R. C. T. 2001 On the orbital response of a rotating cylinder in a current. *Journal of Fluid Mechanics* (in press).